Abruptly Autofocusing Twisted Optical Bottle Beams

You Wu,[1,‡] Zejia Lin,[1,‡] Chuangjie Xu,[1,‡] Danlin Xu,[1] Haiqi Huang,[1] Jiajia Zhao,[1] Zhenwu Mo,[1] Junjie Jiang,[1] Haobin Yang,[1] Liping Zhang,[2] Hongzhan Liu,[1] Dongmei Deng,[1,*] and Lingling Shui[1,†]

[1] *School of Information and Optoelectronic Science and Engineering, South China Normal University, Guangzhou 510006, China*

[2] *School of Physics and Optoelectronic Engineering, Shandong University of Technology, Zibo 255000, China*

(Received 16 December 2021; revised 11 March 2022; accepted 14 April 2022; published 9 May 2022)

Versatile twisted optical bottles (TOBs) generated from a series of abruptly autofocusing beams are derived numerically and experimentally. This kind of TOB beam utilizes dual-autofocus, optical-vortex, and astigmatic phase properties to structure one or more three-dimensional closed dark regions, the bottle space. Closed off-axis multiple optical bottles are generated and observed experimentally. The twist angles can individually affect the rotation of the TOB. The experimental results agree well with our numerical simulations. The relationships between the astigmatic phase, the length of the TOB, the topological order of the vortex, and the width of the TOB are determined. Additionally, stable mesocarbon particles trapped by TOB beams are observed in side view successfully. These TOBs offer more possibilities to trap, sort, and clean microparticles or nanoparticles and improve optical manipulation systems in the future.

DOI: 10.1103/PhysRevApplied.17.054014

I. INTRODUCTION

Optical tweezers, using forces exerted by a strongly focused beam to trap or move microscale-to-nanoscale objects, are ideally suited to manipulating mesoscopic systems [1–6] and play an important role in the fields of biology [7,8], soft-condensed-matter physics [9], and so on. Optical bottle beams, a variant of an optical-tweezer system, form three-dimensional traps by creating low- or null-intensity regions surrounded by a higher intensity [10–12], which enable optical-tweezer systems to trap multiple particles rather than a single one; they may even be useful in high-fidelity quantum simulations and quantum logic operations with Rydberg atoms [13]. Optical bottles are usually produced by on-axis destructive interference of beams [6,14] or caustics under revolution [15], specifically by means of methods such as the self-image effect [16], moiré techniques [6], and Fourier-space generation [17]. The length, the volume, the cross-sectional shape, and the rotation angle are some critical determinants that limit and impact the capability of these bottles to capture particles. How best to alter the determinants for better trapping has become a subject of immense interest. Here, we find that a new method in which abruptly autofocusing beams (AAFBs), after the addition of optical-vortex and astigmatic phase properties, can form a dark region between two autofoci, and, more importantly, can construct well-closed optical bottles with high adjustability.

AAFBs maintain an almost constant low-amplitude profile until a particular focal point, where the AAFB abruptly focuses and, subsequently, the peak intensity increases by orders of magnitude. The laterally inward acceleration before the focal point enables large transverse velocities for radially symmetric beams, and thus the energy can be concentrated [18,19]. The unique feature of a more enhanced longitudinal intensity contrast compared with a typical Gaussian beam leads to potential applications in laser biomedical treatment [18], optical trapping [20–22], generation of light bullets [23], and atom manipulation [24]. The integral functions that satisfy the condition of forming an AAFB originate from higher-order catastrophe theory. A catastrophe is a discontinuous change in the behavior of a function that can occur even when its parameters are varied continuously. In diffraction theory, when higher-order catastrophes appear, rapidly oscillating diffraction integrals containing several control parameters are required; these parameters can represent the light intensity or the quantum mechanical probability density [25–29]. On the other hand, programmable and modulable spatial light modulators (SLMs) allow on-demand loading of phase masks of manifold caustic beams, and can expedite the artificial creation of catastrophe beams in light fields. Artificial low-order catastrophe beams such as Airy beams [30] and Pearcey beams [31] have been successfully

*dengdongmei@m.scnu.edu.cn
†shuill@m.scnu.edu.cn
‡These authors contributed equally.

created and observed. Meanwhile, a high-order optical swallowtail beam, another particular solution of the paraxial Helmholtz equation, has been proposed; it is obtained by mapping the cross sections of the higher-dimensional control-parameter space of swallowtail catastrophes to the corresponding transverse plane [32–34]. Intriguingly, if catastrophes with fold, cusp, and swallowtail geometric structures in the optical field are constrained by a radially symmetric regime, all of them exhibit abruptly autofocusing properties [35–37].

We demonstrate twisted optical bottle beams (TOBBs), a special class of AAFBs exhibiting astigmatism transformation and embedding an optical vortex, whose energy flows through a three-dimensional curved shell, leaving a null-intensity region in the middle. The astigmatism transformation can be effectuated by inserting a cylindrical lens or embedding astigmatic phase information into a phase mask projected onto a SLM [38,39], which allows AAFBs to achieve a dual autofocus and twists the beams so that we can obtain the head and bottom of the bottle. Compared with other conventional bottle beams, TOBBs form optical bottles with better confinement, whose length and twist angle can be also adjusted for better adaptability. The construction of such twisted optical bottles relies on the dynamics of TOBBs, which has potential applications in the particle-manipulation field, such as optical trapping, optical particle sorting, optical particle cleaning, and so on. In this paper, our experimental results are in close agreement with our simulated results.

II. THEORY

In the case of optical catastrophes, there is a well-known classification method for caustic fields, namely the use of the polynomial-generating function $P_n(\mathbf{t}, s)$, which distinguishes various local effects near catastrophes and the system's qualitative behavior [26]:

$$P_n(\mathbf{t}, s) = s^n + \sum_{u=1}^{n-2} t_u s^u, \tag{1}$$

where the control vector $\mathbf{t} = [t_1, t_2, \ldots, t_{n-2}]$ (the t_j are Cartesian coordinates) includes the external control parameters obtained by applying a local transformation (rotations, translations, and rescalings) to the internal state variable s. The polynomial-generating function is inserted into the diffraction integral as a phase item, after which we obtain the diffraction catastrophe integral (DCI), of the form [32,40]

$$C_n(\mathbf{t}) = \int_R \exp\left[iP_n(\mathbf{t}, s)\right] ds. \tag{2}$$

From Eq. (2), we can demonstrate three well-known integrals in paraxial optics, which are the Airy integral $C_3(\mathbf{t}) = \mathrm{Ai}(\mathbf{t}) = \mathrm{Ai}(t_1)$ [41], the Pearcey integral $C_4(\mathbf{t}) = \mathrm{Pe}(\mathbf{t}) = \mathrm{Pe}(t_1, t_2)$ [42], and the swallowtail integral $C_5(\mathbf{t}) = \mathrm{Sw}(\mathbf{t}) = \mathrm{Sw}(t_1, t_2, t_3)$ [32]. These are elementary catastrophes, and each type of caustic catastrophe is characterized by its own form of $P_n(\mathbf{t}, s)$, in which the most significant role is played by the highest-order state variable s^n, called the unfolding of the catastrophe. The C_n in Eqs. (1) and (2) are usually written in Cartesian coordinates, but they can also be expressed in radial coordinates in the optical field. In fact, caustic optical fields expressed as the DCI in radial coordinates have been reported extensively, including the cases of ring Airy beams (the third order of the DCI [18]), ring Pearcey beams (the fourth order of the DCI [31]), ring swallowtail beams (the fifth order of the DCI [32]), and so on. A typical method of transformation is that the first component of the control vector $\mathbf{t}$ in Eq. (1) is considered as the radial-coordinate variable $t_1 = r$, and the other components are directly equal to zero, i.e., $t_2, \ldots, t_{n-2} = 0$. Therefore, the expression for a TOBB in the initial plane in the cylindrical system $(\mathbf{r}, z)$ can be defined for different orders of the DCI and modulated phases as

$$E_n^l(\mathbf{r}, z = 0) = C_n(r)\, D(r)\, V_l(\mathbf{r}) \exp\left[-iA(\mathbf{r})\right], \tag{3}$$

where $\mathbf{r} = (r, \theta)$ is the polar vector. In this paper, we consider the situation $C_3(r) = \mathrm{Ai}(r/p_s w_0)$, $C_4(r) = \mathrm{Pe}(r/p_s w_0, 0)$, $C_5(r) = \mathrm{Sw}(r/p_s w_0, 0, 0)$ [40], where p_s denotes the distribution factor, and w_0 is the beam-waist width of the Gaussian beams.

$$D(r) = \begin{cases} 1, r \le r_0 \\ 0, r > r_0 \end{cases} \tag{4}$$

represents the Heaviside function, which is used in order to ensure that the beam energy is finite. The optical vortex V_l and the astigmatic phase A are the keys to forming optical bottles during propagation:

$$V_l(\mathbf{r}) = \prod_{\mathbf{r}_v} \left(re^{i\theta} + r_v e^{i\theta_v}/w_0\right)^l, \tag{5}$$

$$A(\mathbf{r}) = Rr^2 \sin(\theta - \omega)\cos(\theta - \omega)/w_0^2, \tag{6}$$

where l represents the vortex topological charge, $\mathbf{r}_v = (r_v, \theta_v)$ denotes the position vector of each optical vortex, R is the astigmatic factor, and $\omega \in [0, 2\pi)$ denotes the twist angle. To analyze the propagation properties of TOBBs, we utilize the split-step Fourier-transform method [43] to numerically calculate the three-dimensional optical fields of TOBBs under the paraxial condition.

III. ANALYSIS

Figure 1 displays the phase superimposition process and the initial intensity distributions of astigmatic ring Airy vortex beams (Airy ARVBs, $n = 3$), astigmatic ring

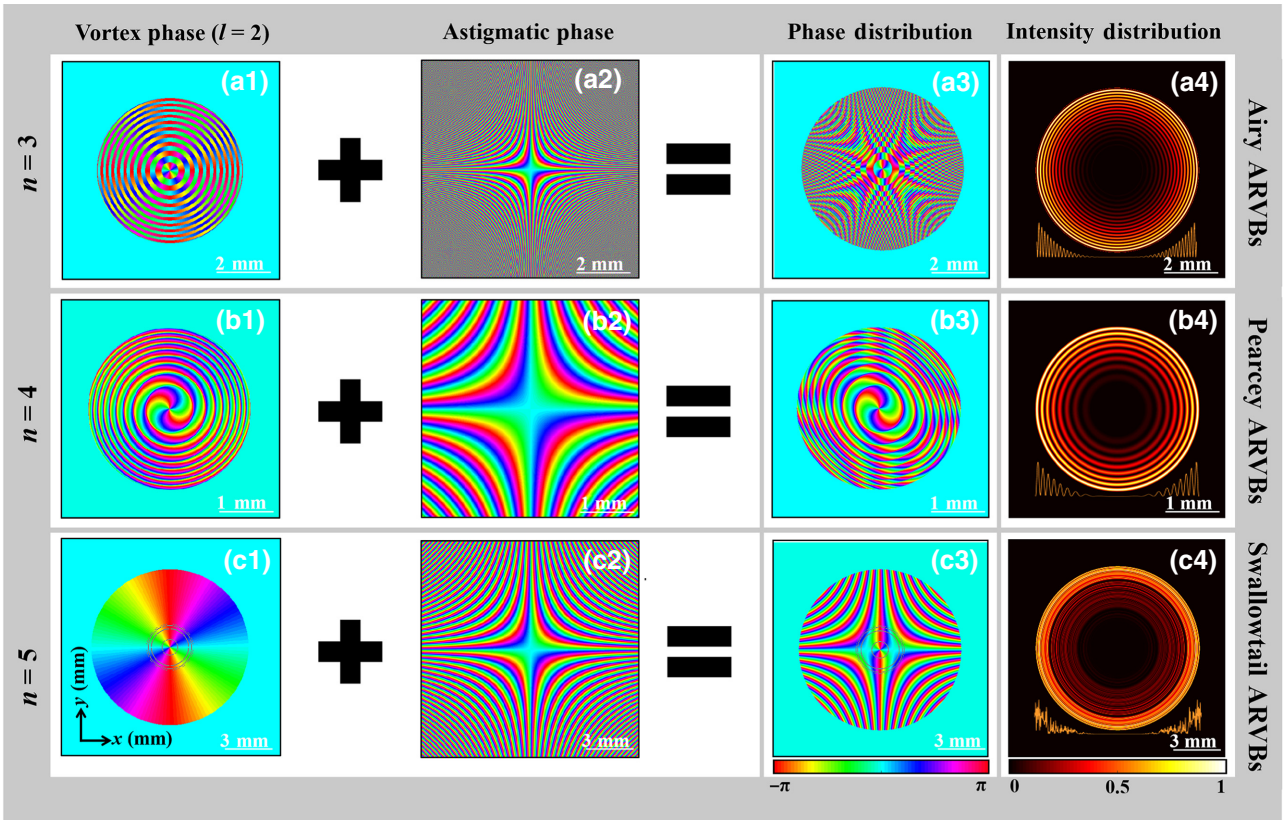

FIG. 1. Phase superimposition processes (a1)–(c3) and initial transverse intensity distributions (a4)–(c4) of TOBBs. The orange curves in (a4)–(c4) are the normalized maximum-intensity distributions as a function of x. We consider the position vector of the vortex $\mathbf{r}_v = (0, 0)$, the twist angle $\omega = 0$, and the beam waist $w_0 = 1.03$ mm, which correspond to the experimental measurement.

Pearcey vortex beams (Pearcey ARVBs, $n = 4$), and astigmatic ring swallowtail vortex beams (swallowtail ARVBs, $n = 5$), obtained by setting appropriate regulatory factors [Figs. 1(a1)–1(a4), $p_s = 0.2$, $R = 12$; Figs. 1(b1)–1(b4), $p_s = 0.1$, $R = 10$; Figs. 1(c1)–1(c4), $p_s = 800$, $R = 3$] to form the TOBs. There are two key phase components for forming TOBBs: the astigmatic phase and the vortex phase. Under the influence of the astigmatic phase [38], the rings of the TOBBs are elongated in the direction of $x = -y$. From Figs. 1(a1)–1(a3), each ring of the Airy phase in the cylindrical system truncates the astigmatic phase and produces a spatial phase transition. It can be seen from Figs. 1(b1)–1(b3) that several circles composed of phase-mutation lines generated by the Pearcey phase are stretched into an ellipse by the astigmatic phase. In addition, in Figs. 1(c1)–1(c3), the ring swallowtail phase and the astigmatic phase do not blend so obviously. Concentrating on the phase distributions and superimposition, we find that the astigmatic phase can be better integrated into the ring Pearcey vortex phase, as shown in Figs. 1(b1)–1(b3). Because of the discrepancies in the phase distributions, these phases can generate versatile TOBs, as shown in the next section. From Figs. 1(a4)–1(b4), this makes it clear that the optical fields of these three types of TOBBs with different orders of the DCI have homogeneous intensity distributions in the initial plane. The intensity distributions of the Airy ARVBs and Pearcey ARVBs have distinct oscillation curves and rings. Nevertheless, the rings of the swallowtail ARVBs are thin and densely distributed, so that their curves have very uneven oscillations along the radial axis.

Next, we analyze the TOBs formed by three such kinds of beams propagating in free space, as displayed in Fig. 1. Although TOBBs are not Gaussian-like beams, it is necessary for us to utilize Gaussian beams to experimentally generate the TOBBs we need. Therefore, we use the Rayleigh distance $z_R = 0.5kw_0^2$ as a propagation-distance scale in the z direction. By adjusting the structure of the TOBBs, we can create a TOB in free space, which has a practically closed three-dimensional null-intensity space enclosed by a higher intensity. Similarly to Refs. [38,44,45], the head and the bottom of the TOB are formed in the two planes with the highest intensities. These three beams all keep their radial symmetry in the initial plane, and then focus automatically into an elongated lobe on the line $y = -x$ in the head plane, as shown in Figs. 2(a2)–2(c2). However, the further evolution of these beams is very different. From Fig. 2(a1), due to the angular

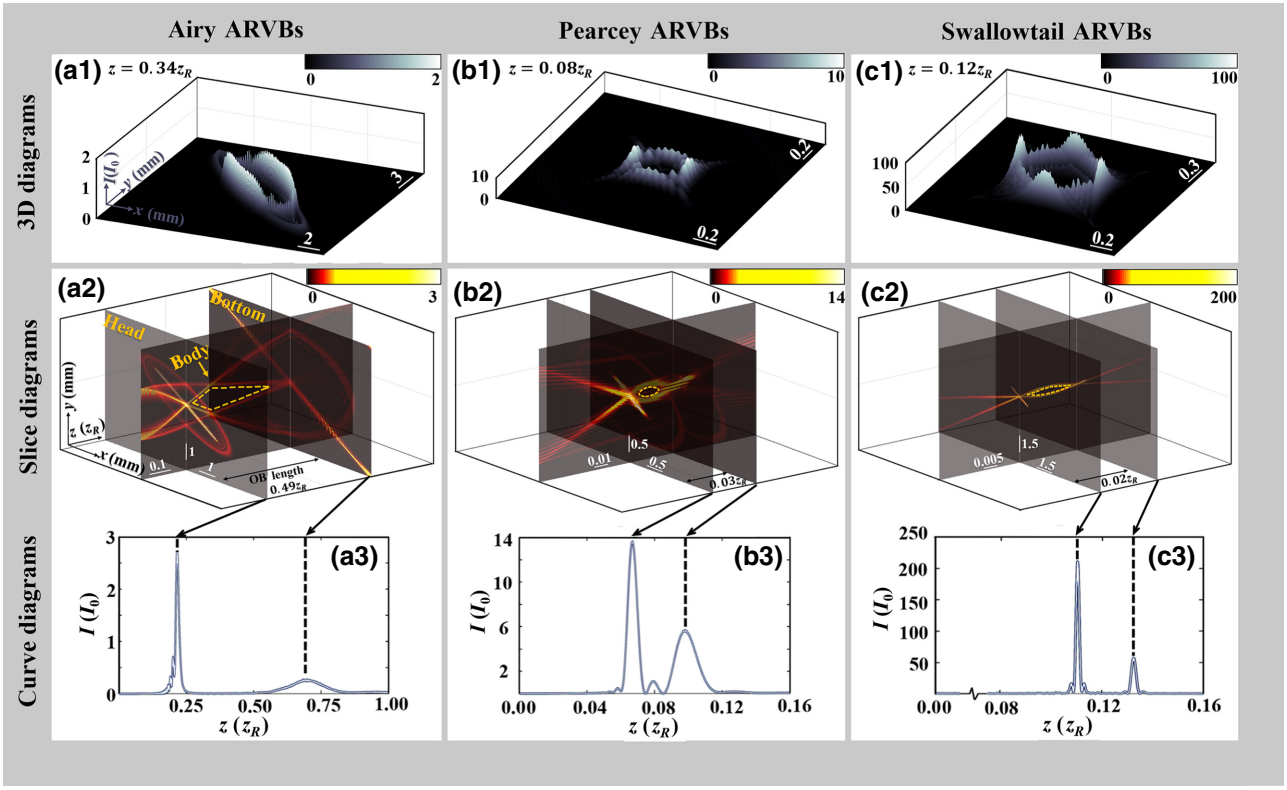

FIG. 2. Intensity distributions [three-dimensional (3D) transverse-intensity-distribution diagrams, propagation-slice diagrams, and intensity curves along the z axis] of TOBBs with different orders of the DCI, propagating in free space: (a1)–(a3) $n = 3$; (b1)–(b3) $n = 4$; (c1)–(c3) $n = 5$. The other parameters are the same as in Fig. 1.

momentum of the optical vortex, the linear distribution of the beams slowly transforms into a closed elliptical-ring shape during propagation. Then, the main lobe turns into a boatlike shape with a relatively low intensity distribution at both ends, until the second focus of the Airy ARVB, at which point it closes again to form the bottom of the bottle. The lobe at the bottle bottom is presumably 2 times wider along the line $y = -x$ than that at the head of the bottle. By observing the intensity distribution along the z axis in Fig. 2(a3), we can measure the length of the TOB according to the relative position of the two focusing planes. We discuss the measurement of the TOB length further in Sec. IV. The TOB formed by the Airy ARVBs is the longest one, but it is surrounded by the lowest normalized intensity, which forms the bottle wall of the TOB. The TOB generated by the Pearcey ARVBs is the most representative. The dynamics of such propagation behavior can be clearly visualized in Figs. 2(b1)–2(b3). In the plane $z = 0.08z_R$, we find that the intensity pattern gradually transforms into a rhombuslike structure with elliptical rings outside until the second focus is reached, which is shown in Fig. 2(b1). The main lobe of the Pearcey ARVB in the bottom plane is distributed along the line $y = x$, which is rotated by $\pi/2$ compared with that for the head plane. The position $z = 0.08z_R$ is at approximately the center of the 90° twist rotation from the head plane to the bottom plane. There is a phenomenon of inversion here, caused by the essence of the Pearcey function. The spot patterns of the transverse sections of Pearcey beams are upside down before and after focusing, which is the "self-inversion" property [31]. Because of the complex phase modulation, "self-inversion" of Pearcey ARVBs happens between the first and the second focal plane. Therefore, the spot is not elongated in this plane, and it is elongated in the first and the third quadrants after this plane [Fig. 2(b2)]. Differently from the other two kinds of beams, Fig. 2(b3) shows that there is a small intensity peak at the center during the propagation of Pearcey ARVBs from the head plane to the bottom plane. The length of the TOBs formed by the Pearcey ARVBs is far smaller than that for the Airy ARVBs, but the Pearcey ARVBs provide a stronger "particle cage" for optical manipulation. Finally, we concentrate on the case of swallowtail ARVBs, with $n = 5$. Generally, when working with this kind of TOBB ($n = 5$), it is difficult to guarantee a certain minimum distance between the two foci, which is needed to form a TOB in Figs. 2(a2) and 2(b2). In order to do so, we need to embed an additional quadratic phase $[\exp[-iQ(x^2 + y^2/w_0^2)]$; Q is the quadratic factor, which we set to 16.55] in the initial plane of the swallowtail ARVBs so that the two focal planes can

be separated by a certain distance, as shown in Fig. 2(c2). In fact, the quadratic factor is physically equivalent to the ratio of the Rayleigh length to the focal length of a spherical lens. In this situation, the inversion in the bottom plane is caused by the lens. The swallowtail ARVBs generate the smallest TOB with the highest intensity, which is the most stable way to hold particles [46]. Therefore, in a hypothetical concept, OB beams with a dual autofocus can also be utilized in optical cloaking [47], as they can avoid obstacles or detectors during propagation and can autofocus with no change along the propagation direction. In this situation, we need not mechanically adjust the optical device to avoid these obstacles. Instead, we need only to calculate the corresponding parameters of the beams and load the corresponding information into a SLM to avoid an object.

To demonstrate the twisted behavior of TOBBs, we introduce a twist-angle variable ω. By adjusting the twist angle ω, we can obtain different twisted shapes of the TOB. Because of the self-inversion property, we choose the most typical kind of TOBBs, generated by Pearcey ARVBs, to discuss the distinctions that can be obtained by changing the twist angle. Figure 3 shows the intensity distributions from the first autofocusing plane (the TOB head, $z = 0.07z_R$) to the second autofocusing plane (the TOB bottom, $z = 0.10z_R$). The angle does not affect the length and volume of the bottle. In the above discussion and in Figs. 2(b1)–2(b3), when $\omega = 0$, the main lobe of the Pearcey ARVBs is distributed along the line $y = -x$, which is at an angle of approximately 45° with respect to the x axis. In Figs. 3(b) and 3(c), when the twist angle ω is adjusted to 45° and 60°, the distribution pattern in the first focal plane (the head plane) is transformed into lines at angles of 0° and 15°, respectively. In general, the main lobes in the head plane and the bottom plane of Pearcey ARVBs with a twist angle ω are distributed along the lines $y/x = \arctan(\omega - \pi/4)$ and $y/x = \arctan(\omega + \pi/4)$, respectively. With these general formulas, we can obtain a TOB with the predesigned twisted shape that we need.

The vortex topological charge l also plays an important role in modulating the shape of OB beams [38]. A scattering diagram of the largest width along the x axis for TOBs formed from beams with different charges ($l = 1, 2, \ldots, 7$) propagating in free space is clearly shown in Fig. 4. The width of a TOB is dominated by the vortex topological charge. The almost monotonically increasing solid line in Fig. 4(a) illustrates that the topological charge is positively correlated with the width of the TOB. More importantly, the phenomenon of bright and dark spots at the focus point is related to the parity of the vortex order [48]. A bright spot appears in the focal plane when the order of the vortex is even, which can be utilized to structure a closed OB. As shown in Figs. 4(b1) and 4(b2), TOBBs with a high-even-order vortex still maintain a bright spot in the focal plane. Nevertheless, it is not advantageous to blindly increase the vortex order. An increase in the vortex topological charge

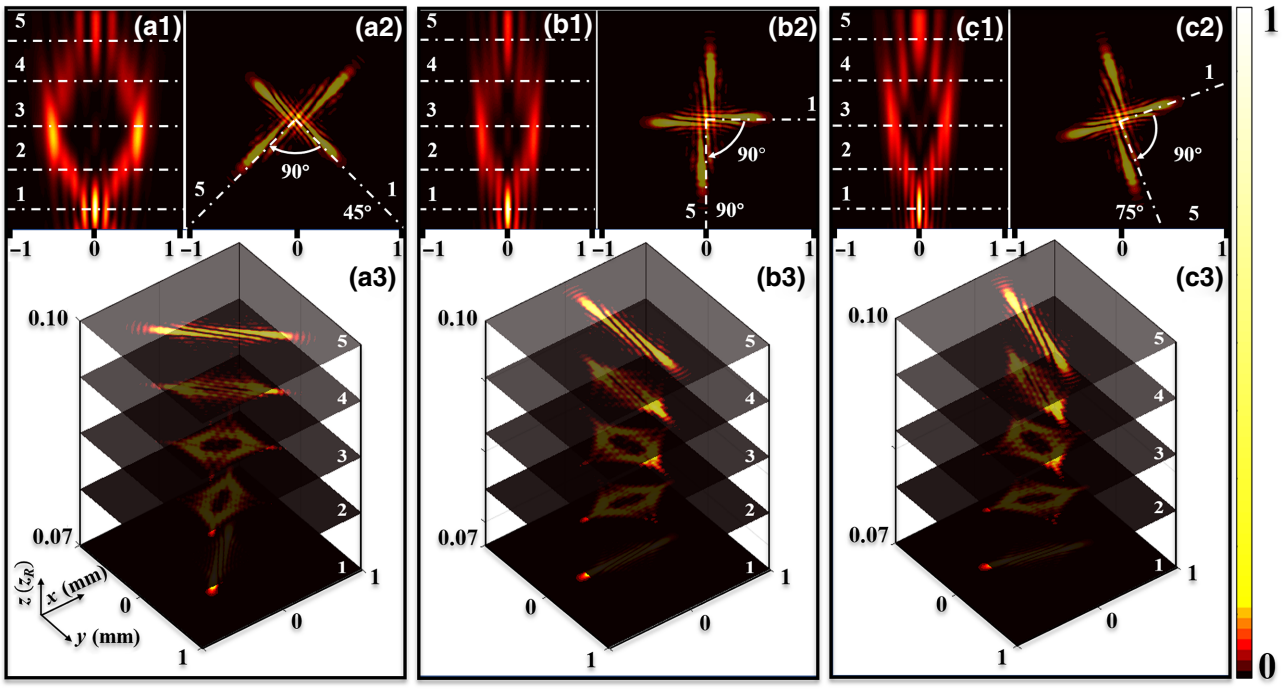

FIG. 3. Intensity distributions of Pearcey ARVBs with different twist angles ($\omega = 0$, $\omega = \pi/4$, and $\omega = \pi/3$): (a1)–(c1) side views of the TOB in the $x = (y - z)$ plane; (a2)–(c2) heads and bottoms of the bottles; (a3)–(c3) slice diagrams. The other parameters are the same as in Fig. 1(b).

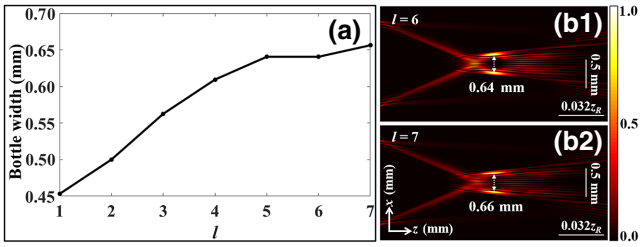

FIG. 4. (a) Maximum TOB width along the x axis versus vortex topological charge; (b1),(b2) side views of propagation of Pearcey ARVBs with $l = 6$ and $l = 7$, respectively. The other parameters are the same as in Fig. 1(b).

leads to more serious spot splitting, and so the beam cannot form a relatively closed dark region. In our simulation, we find that the TOBBs in the case $l = 2$ show the best bottle structure.

IV. EXPERIMENT

In the study presented in this paper, we generate TOBBs by means of holographic imaging [49], which is a popular method in the field of spatial light generation [19,21,30,32,33,37,50–53]. Because spatial-light-modulation technology is already mature and widely used, we draw on experience from previous research and establish the experimental scheme shown by the 3D model in Fig. 5. The fundamental transverse Gaussian mode is emitted by a power-adjustable

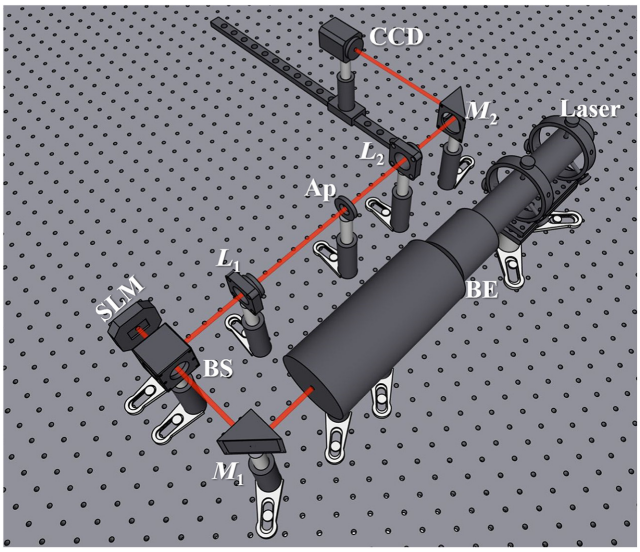

FIG. 5. Experimental scheme: power-adjustable laser ($\lambda = 532$ nm, power range from 1 mW to 6 W); BE, eightfold beam expander; M_1, M_2, mirrors; SLM, reflective spatial light modulator (Santec SLM-200); BS, beam splitter; CCD, charge-coupled device (BeamPro 11.11). The $4f$ optical filter system consists of two thin lenses L_1 ($f_1 = 300$ mm) and L_2 ($f_2 = 300$ mm) and an aperture Ap.

laser ($\lambda = 532$ nm). We use an eightfold beam expander to collimate and expand the Gaussian beam, so that the beam is reflected from the SLM in such a way that it carries sufficient information. After the beam passes through the beam splitter, a $4f$ spatial filter filters out all the interference fringes except for the $+1$ order in the spectrum plane. Finally, we obtain the initial intensity distribution of the TOBB in the image focal plane of L_2. By moving the CCD camera on a slide slowly and steadily, we can observe the propagation phenomena of the TOBB. We measure and calculate the final beam waist $w_0 = 1.03$ mm in the focal plane of L_2.

Basically, the intensity distributions measured by the CCD in the experiment [Figs. 6(a1)–6(c4)] for these three types of TOBBs are practically consistent with the distributions in the simulation shown in Fig. 2. The Airy ARVBs have two solid spots in the center of the head plane as well as in the bottom plane, and they provide a closed zero-light dark region, as shown in Fig. 6(a3). The Pearcey ARVBs maintain the typical propagation-inversion property. The distribution in the head plane [Fig. 6(b2)] is similar to the distribution in the bottom plane [Fig. 6(b4)] after the application of mirror symmetry. The needle-shaped spot is rotated by 90°. From Figs. 6(c1)–6(c4), the swallowtail ARVBs do not have the inversion property. When the astigmatic factor R is very small, the second focus is too far from the first focus to form a TOB. Diffraction expands the beam rapidly, so that the intensity is very weak when the swallowtail ARVB propagates to the second focal plane. Additionally, as we have mentioned above, if R is too large, due to the very intense focus of ring swallowtail beams, the two focal planes are too close together to form a TOB. It is hard to apply this kind of too large and weak-intensity or too small and strong-intensity TOB without a quadratic phase. On the other hand, with a quadratic phase in the SLM, it is hard to choose pure $+1$ fringes in the $4f$ system, because the orders of the interference fringes are very close to each other. To solve these problems, we use a focusing lens that replaces the quadratic phase ($k/2f = Q/w_0^2$, where the focal length of the lens is $f = 300$ mm) equivalently in the initial plane (the image focal plane of L_2) to adjust the position of the second focal plane. In this case, we can obtain an appropriate TOB from a swallowtail ARVB during propagation.

The astigmatic factor R also has a positive correlation with the length of the TOB. We present a discussion of the relationship between the astigmatic phase and the TOB length in Fig. 7. We select 11 different astigmatic factors, equally spaced within the interval [7, 12]. As shown by the two scatter polylines in Fig. 7(b), we experimentally measure (the blue solid line) and numerically calculate (the red dashed line) the positions of the head and the bottom of the bottle [the reference intensity distribution can be seen in Figs. 7(a1) and 7(a2)] to obtain the TOB length. After eliminating the undulations caused by laser diffraction,

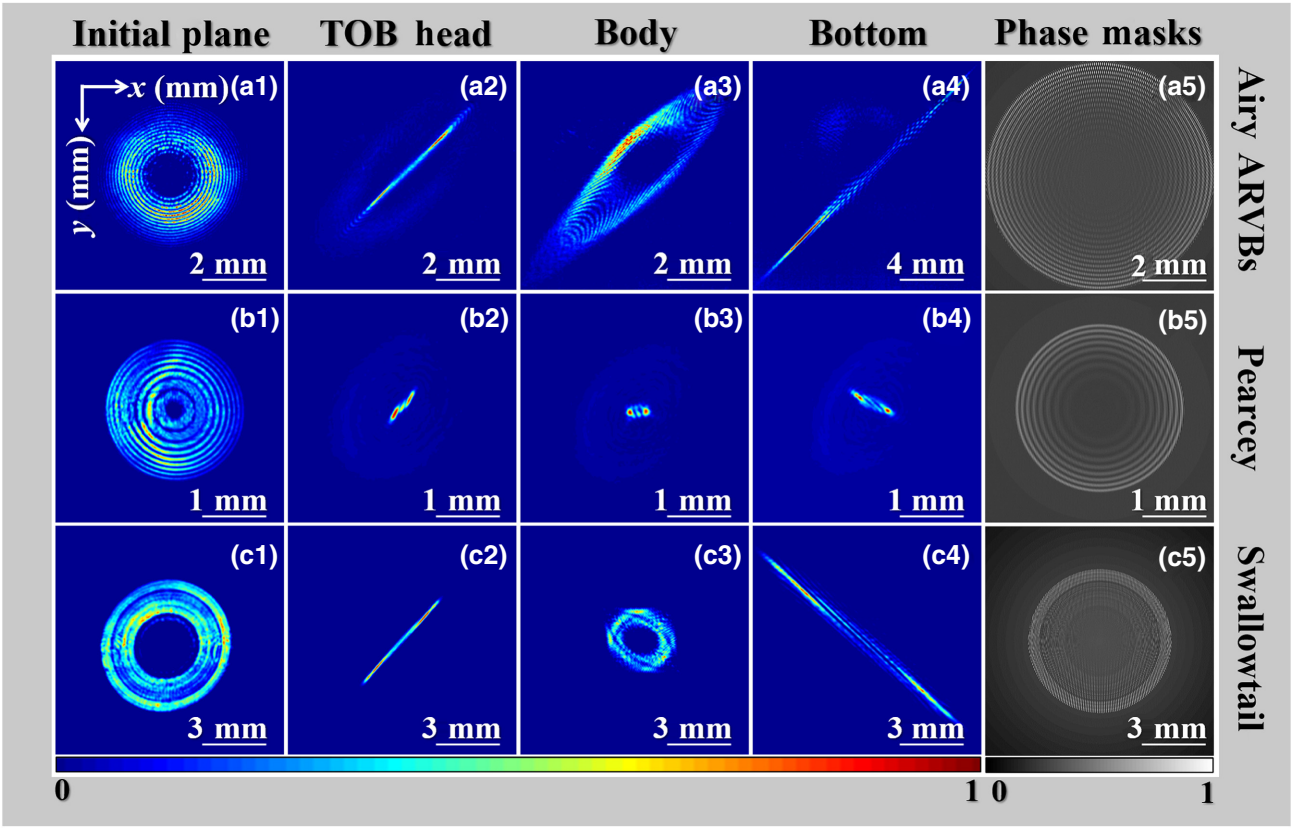

FIG. 6. Experimental snapshots of normalized intensity distributions in the initial plane, the head plane, the body plane, and the bottom plane, and the phase masks of the TOBBs: (a1)–(a5) Airy ARVBs; (b1)–(b5) Pearcey ARVBs; (c1)–(c5) swallowtail ARVBs. The parameters are the same as in Fig. 1.

interference, air turbulence, and dust, the results of the simulation calculations and experimental measurements are very consistent. However, we cannot just keep increasing R to infinity or a very large value, because of the practical image limit (phase mask) of the SLM (up to approximately 25 in our experimental method). Another negative factor is that the intensity is attenuated due to diffraction, which means that if the bottle length is too large, the intensity at the bottom of the bottle is too weak to trap particles.

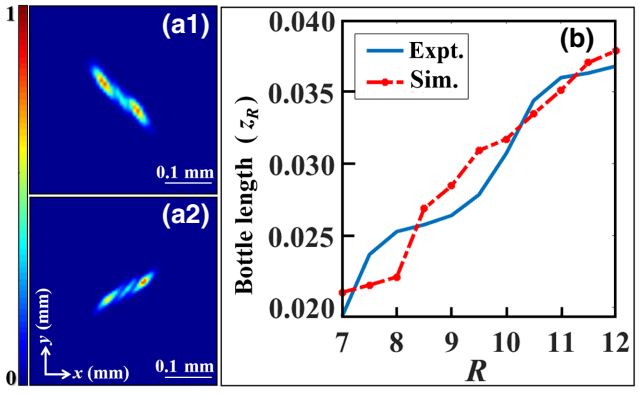

FIG. 7. (a1),(a2) Experimental intensity distributions of Pearcey ARVBs observed with the CCD in the TOB head plane and bottom plane, respectively; (b) TOB length versus astigmatic factor in the simulation and experiment. The other parameters are the same as in Fig. 1(b).

Next, after analyzing the relationship between the astigmatic factor and the bottle length, we can start to obtain more complex-structured TOBBs. Recently, a class of highly controllable complex-structured beams, namely beams for off-axis multiple optical bottles (OMOBs), has been theoretically investigated. [38,45,54–56]. This kind of OMOB is a product of beam propagation in free space, utilizing multiple autofocuses and off-axis optical vortices to form a complicated light-field structure. The complicatedly structured beams have several closed zero-intensity spaces that can be used for "particle cages." Such complex-structured beams can be easily generated by calculating the phase mask that is used in the SLM. We continue to use the experimental scheme shown in Fig. 5 to generate off-axis multiple TOBs. Here, we generalize and observe off-axis multiple TOBs obtained from TOBBs in the experiment. Figure 8 demonstrates the propagation dynamics of Pearcey ARVBs with two off-axis optical vortices. These two off-axis vortices are the key to generating such

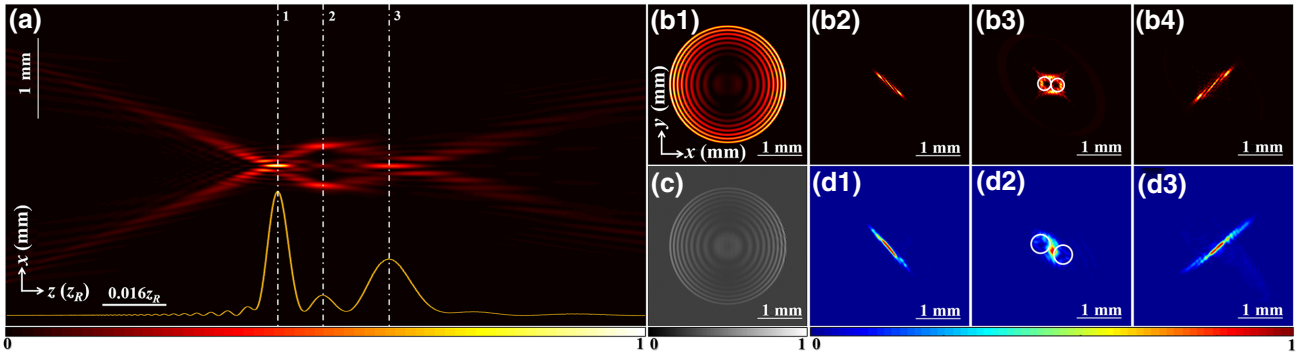

FIG. 8. Off-axis multiple TOBs formed by Pearcey ARVBs with two different off-axis optical vortices with $l = 2$, $\mathbf{r}_{v1} = (r_{v1}, \theta_{v1}) = (0.45, \pi/2)$, and $\mathbf{r}_{v2} = (r_{v2}, \theta_{v2}) = (0.45, -\pi/2)$]: (a) numerically simulated side view of Pearcey ARVBs propagating in free space; (b1) numerically simulated transverse intensity patterns in the initial plane; (b2)–(b4) numerically simulated transverse intensity patterns in the planes 1–3 marked in (a); (c) phase mask; (d1)–(d3) experimental transverse intensity patterns corresponding to (b2)–(b4). Two off-axis bottle spaces are marked by white circles. The other parameters are the same as in Fig. 1(b).

complex OMOBs. A dark region is caused by an optical vortex. Therefore, if the position of the vortex changes and the number of vortices is increased, we obtain an OMOB. The result in Fig. 8 is obtained by increasing N to 2 and using two off-axis symmetric optical vortices along the y axis ($x = 0, y = \pm 0.45$ mm). Compared with the situation of one on-axis vortex, the body of the TOB seems to be divided into two off-axis bottle spaces, which are marked by white circles. Regarding the generation of OMOBs, we have a great improvement toward solving the problem that the characteristics of OBs are difficult to efficiently control by varying the beam-focusing conditions [57]. We have to choose the topological charge or the positions of the vortices within an appropriate range, which means that the number and the positions of the vortices have a maximum limitation ($N < 7$ and $r < 1$ mm), or we obtain several incompletely enclosed bottle spaces. In the appropriate range, we can change the position and the shape of each TOB, and there is no doubt that we can get three, four, or even five off-axis multiple TOBs. From Fig. 8, this means that highly tunable OMOBs can be generated in a real experiment, which may offer more possibilities for trapping microparticles or nanoparticles in the future.

Finally, we utilize a simple experimental setup to verify the photophoretic trapping properties of the TOBBs. Stable trapping and manipulation of light-absorbing particles can be experimentally achieved with a bottlelike structure [58]. The laser beams radiate heat, and the heated gas molecules exchange linear momentum with a particle, which generates a force that pushes the particle. Figure 9 shows results obtained with Pearcey ARVBs as a typical beam sample (approximately 6 W output laser power) after constriction incidence into a glass cuvette (10 mm × 10 mm × 40 mm) containing absorbing carbon particles of median size $D_{50} = 23.83 \times 10^{-3}$ mm. The position of generation of the TOBBs in Fig. 9(a) is in the image focal plane of L_2 shown in Fig. 5. Before observing the trapping phenomenon, we shake the cuvette in order to assist the TOBBs in trapping the particles. The mechanism of observation is shown in the inset of Fig. 9(a). Because of the dark region, the particles inside it do not scatter light. Only trapped particles touching the TOB wall can

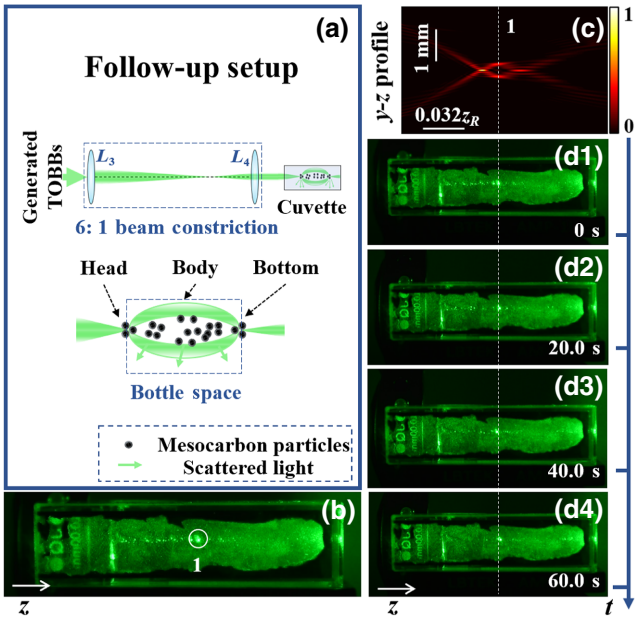

FIG. 9. (a) Schematic diagrams of the follow-up experimental setup and particle trapping for mesocarbon microbeads; the 6× beam-constriction system consists of two thin lenses L_3 ($f_3 = 150$ mm) and L_4 ($f_4 = 25.4$ mm); (b) side view of the glass cuvette, in which light is scattered from Pearcey ARVBs that trap the particles; (c) numerically simulated side view of Pearcey ARVBs propagating in free space; (d1)–(d4) photographs of the glass cuvette taken from the side at 20-s intervals. The complete process, with a duration of about 3 min, is shown in the Supplemental Material [59]. The parameters are the same as in Fig. 1(b).

scatter light. If the particles are trapped in the bottle, the light scattered by the particles near the bottle wall causes several stable small bright spots, which are marked by a white circle in Fig. 9(b). As shown in the video file (See Supplemental Material [59]), a small bright spot is stable in the middle of the cuvette. Similarly to Refs. [60,61], this phenomenon proves that the TOB can capture particles stably for a few minutes. Moreover, several carbon particles may oscillate back and forth along the propagation axis because the size of the particles causes different collision strengths of gas molecules with different particle surfaces [62,63]. Figures 9(d1)–9(d4) are side-view photographs of the glass cuvette taken at 20-s intervals. The positions of the TOB agree well with the simulation. The particles can be trapped for a certain time, which means that robust and stable TOBs can be formed. If we use a laser source with a low power, the particles can easily oscillate due to environmental disturbances. At the same time, the particles are affected not only by the optics, but also by gravity in the vertical direction. The longer the time is, the fewer particles there are that can be captured stably. This situation can be alleviated well by trapping particles in a solution, because the buoyancy of the solution can offset gravity. Because of perturbations, several carbon particles are out of focus, or they have moved to areas where there is no light. In addition, when other particles are trapped in the interior of the TOB, the dark region cannot reflect any light to the observer. We need to build a side-view observation system with another light source, with a different wavelength and objective lens. In addition, compared with most optical-tweezer experiments [20,64], the captured particles are observed at a certain propagation distance, and so we need to change the observation plane to a different position by moving the whole observation system, which causes external oscillations and disturbance. The method that we use in this paper can intuitively and conveniently help us observe the trapping of particles in the longitudinal propagation direction, but this is at the expense of accuracy. A direct method would be to greatly increase the power of the laser source, so as to provide a greater capture force to trap particles more stably.

V. CONCLUSION

In summary, we introduce a kind of structured beam, abruptly autofocusing TOBBs, which form one or several closed zero-light spaces during propagation. The closed dark region of the TOB provides a stronger "particle cage" for optical manipulation. Compared with the results of previous research on optical bottles, more complicated structures can be generated, and these can be manipulated simply by changing the beam parameters, without any mechanical scanning. We combine three types of optical beams with singularities in cylindrical coordinates and compare them. Airy ARVBs form the largest TOBs but with the weakest focal intensity. Pearcey ARVBs are the most typical type of beam, with a larger focal intensity and a more complex structure. Swallowtail ARVBs have the strongest focal intensity but need a lens to form a TOB. We discuss the influences of the twist angle, the vortex topological charge, and the astigmatic factor on the shape of TOBs. Our experimental results correspond well to our numerical results. The particle-trapping experiment exhibits a stable and robust TOB in air. Besides, we also discuss the possibility of using TOBBs to realize optical particle sorting and optical particle cleaning, which is a basic step in improving multiparticle manipulation.

ACKNOWLEDGMENTS

This work was supported by the National Natural Science Foundation of China (Grants No. 12174122 and No. 11775083), the Science and Technology Program of Guangzhou (Grant No. 2019050001), and the Extracurricular Scientific Program of the School of Information and Optoelectronic Science and Engineering, South China Normal University (Grant No. 21GDKB02).

We declare that we have no conflict of interest. Dr. Chuangjie Xu is currently with Sun Yat-Sen University.

[1] D. G. Grier, A revolution in optical manipulation, Nature **424**, 810 (2003).
[2] Y. J. Yang, Y. X. Ren, M. Z. Chen, Y. Arita, and C. Rosales-Guzmán, Optical trapping with structured light: A review, Adv. Photonics **3**, 034001 (2021).
[3] K. Svobodaand and S. M. Block, Optical trapping of metallic Rayleigh particles, Opt. Lett. **19**, 930 (1994).
[4] L. P. Ghislain, N. A. Switz, and W. W. Webb, Measurement of small forces using an optical trap, Rev. Sci. Instrum. **65**, 2762 (1994).
[5] F. Gittesand and C. F. Schmidt, Signals and noise in micromechanical measurements, Methods Cell Biol. **55**, 129 (1998).
[6] P. Zhang, Z. Zhang, J. Prakash, S. Huang, D. Hernandez, M. Salazar, D. N. Christodoulides, and Z. Chen, Trapping and transporting aerosols with a single optical bottle beam generated by moiré techniques, Opt. Lett. **36**, 1491 (2011).
[7] R. X. Zhu, T. Avsievich, A. Popov, and I. Meglinski, Optical tweezers in studies of red blood cells, Cells **9**, 545 (2020).
[8] A. Ashkin, J. M. Dziedzic, and T. Yamane, Optical trapping and manipulation of single cells using infrared-laser beams, Nature **330**, 769 (1987).
[9] A. P. Chikkatur, Y. Shin, A. E. Leanhardt, D. Kielpinski, E. Tsikata, T. L. Gustavson, D. E. Pritchard, and W. Ketterle, A continuous source of Bose-Einstein condensed atoms, Science **296**, 2193 (2002).
[10] A. Ashkin, Acceleration and Trapping of Particles by Radiation Pressure, Phys. Rev. Lett. **24**, 156 (1970).

[11] R. Ozeri, L. Khaykovich, and N. Davidson, Erratum: Long Spin Relaxation Times in a Single-Beam Blue-Detuned, Phys. Rev. Lett. **59**, R1750 (1999).

[12] P. Xu, X. D. He, J. Wang, and M. S. Zhan, Trapping a single atom in a blue detuned optical bottle beam trap, Opt. Lett. **35**, 2164 (2010).

[13] D. Barred, V. Lienhar, P. Scholl, S. de Léséleuc, T. Boulier, A. Browaeys, and T. Lahaye, Three-Dimensional Trapping of Individual Rydberg Atoms in Ponderomotive Bottle Beam Traps, Phys. Rev. Lett. **124**, 023201 (2020).

[14] P. Rudy, R. Ejnisman, A. Rahman, S. Lee, and N. P. Bigelow, An all optical dynamical dark trap for neutral atoms, Opt. Express **8**, 159 (2001).

[15] I. Chremmos, Z. G. Chen, D. N. Christodoulides, and N. K. Efremidis, Abruptly autofocusing and autodefocusing optical beams with arbitrary caustics, Phys. Rev. A **85**, 023828 (2012).

[16] B. P. S. Ahluwalia, X. C. Yuan, and S. H. Tao, Transfer of 'pure' on-axis spin angular momentum to the absorptive particle using self-imaged bottle beam optical tweezers system, Opt. Express **12**, 5172 (2004).

[17] I. Chremmos, P. Zhang, J. Prakash, N. K. Efremidis, D. N. Christodoulides, and Z. Chen, Fourier-space generation of abruptly autofocusing beams and optical bottle beams, Opt. Lett. **36**, 3675 (2011).

[18] N. K. Efremidisand and D. N. Christodoulides, Abruptly autofocusing waves, Opt. Lett. **35**, 4045 (2010).

[19] D. G. Papazoglou, N. K. Efremidis, D. N. Christodoulides, and S. Tzortzakis, Observation of abruptly autofocusing waves, Opt. Lett. **36**, 1842 (2011).

[20] P. Zhang, J. Prakash, Z. Zhang, M. S. Mills, N. K. Efremidis, D. N. Christodoulides, and Z. G. Chen, Trapping and guiding microparticles with morphing autofocusing Airy beams, Opt. Lett. **36**, 2883 (2011).

[21] Y. F. Jiang, Z. L. Cao, H. H. Shao, W. T. Zheng, B. X. Zeng, and X. H. Lu, Trapping two types of particles by modified circular Airy beams, Opt. Express **24**, 18072 (2016).

[22] Y. J. Shen, X. J. Wang, Z. W. Xie, C. J. Min, X. Fu, Q. Liu, M. L. Gong, and X. C. Yuan, Optical vortices 30 years on: OAM manipulation from topological charge to multiple singularities, Light: Sci. Appl. **8**, 90 (2019).

[23] P. Panagiotopoulos, D. G. Papazoglou, A. Couairon, and S. Tzortzakis, Sharply autofocused ring-Airy beams transforming into non-linear intense light bullets, Nat. Commun. **4**, 2622 (2013).

[24] N. K. Efremidis, V. Paltoglou, and W. Klitzing, Accelerating and abruptly autofocusing matter waves, Phys. Rev. A **87**, 043637 (2013).

[25] V. I. Arnold, *Catastrophe Theory* (Springer-Verlag, Berlin Heidelberg, 1984).

[26] M. V. Berryand and C. Upstill, Iv catastrophe optics: Morphologies of caustics and their diffraction patterns, Prog. Opt. **18**, 257 (1980).

[27] J. A. Lockand and J. H. Andrews, Optical caustics in natural phenomena, Am. J. Phys. **60**, 397 (1992).

[28] R. Borghi, Evaluation of cuspoid and umbilic diffraction catastrophes of codimension four, J. Opt. Soc. Am. A **28**, 887 (2011).

[29] E. Zeleny, Canonical integrals for diffraction catastrophes (2014), https://demonstrations.wolfram.com/CanonicalIntegralsForDiffractionCatastrophes/.

[30] G. A. Siviloglou, J. Broky, A. Dogariu, and D. N. Christodoulides, Observation of Accelerating Airy Beams, Phys. Rev. Lett. **99**, 213901 (2007).

[31] J. D. Ring, J. Lindberg, A. Mourka, M. Mazilu, K. Dholakia, and M. R. Dennis, Auto-focusing and self-healing of Pearcey beams, Opt. Express **20**, 18955 (2012).

[32] A. Zannotti, F. Diebel, and C. Denz, Dynamics of the optical swallowtail catastrophe, Optica **4**, 1157 (2017).

[33] A. Zannotti, F. Diebel, M. Boguslawski, and C. Denz, Optical catastrophes of the swallowtail and butterfly beams, New J. Phys. **19**, 053004 (2017).

[34] H. A. Teng, Y. X. Qian, Y. P. Lan, and W. T. Cui, Swallowtail-type diffraction catastrophe beams, Opt. Express **29**, 3786 (2021).

[35] X. Y. Chen, D. M. Deng, J. L. Zhuang, X. Peng, D. D. Li, L. P. Zhang, F. Zhao, X. B. Yang, H. Z. Liu, and G. H. Wang, Focusing properties of circle Pearcey beams, Opt. Lett. **43**, 3626 (2018).

[36] X. Y. Chen, D. M. Deng, G. H. Wang, X. B. Yang, and H. Z. Liu, Abruptly autofocused and rotated circular chirp Pearcey Gaussian vortex beams, Opt. Lett. **44**, 955 (2019).

[37] H. A. Teng, Y. X. Qian, Y. P. Lan, and Y. M. Cai, Abruptly autofocusing circular swallowtail beams, Opt. Lett. **46**, 270 (2021).

[38] Y. Wu, Z. J. Lin, C. J. Xu, X. M. Fu, K. H. Chen, H. X. Qiu, and D. M. Deng, Off-axis and multi optical bottles from the ring Airy Gaussian vortex beam with the astigmatic phase, Ann. Phys. **532**, 2000188 (2020).

[39] M. W. Beijersbergen, L. Allen, H. E. L. O. van der Veen, and J. P. Woerdman, Astigmatic laser mode converters and transfer of orbital angular momentum, Opt. Commun. **96**, 123 (1993).

[40] J. F. Nye, *Natural Focusing and Fine Structure of Light: Caustics and Wave Dislocations* (Institute of Physics, Philadelphia, 1999).

[41] O. Vallée and M. Soares, *Airy Functions and Applications to Physics* (World Scientific, London, 2010).

[42] T. Pearcey, XXXI. The structure of an electromagnetic field in the neighbourhood of a cusp of a caustic, Lond., Edinb., Dublin Philos. Mag. J. Sci. **37**, 311 (1946).

[43] T. C. Poonand and T. Kim, *Engineering Optics With MATLAB Pub Co Inc* (World Scientific, Singapore, 2006).

[44] L. P. Zhang, D. M. Deng, X. B. Yang, G. H. Wang, and H. Z. Liu, Effects of the modulated vortex and second-order chirp on the propagation dynamics of ring Pearcey Gaussian beams, Opt. Lett. **44**, 4654 (2019).

[45] C. J. Xu, Y. Wu, and D. M. Deng, Multioptical bottles from second-order chirped symmetric Airy vortex beams, Opt. Lett. **45**, 3502 (2020).

[46] K. Okamotoand and S. Kawata, Radiation Force Exerted on Subwavelength Particles Near a Nanoaperture, Phys. Rev. Lett. **83**, 4534 (1999).

[47] A. Y. Bekshaev, M. S. Soskin, and M. V. Vasnetsov, Optical cloaking with metamaterials, Nat. Photonics **1**, 224 (2007).

[48] A. Y. Bekshaev, M. S. Soskin, and M. V. Vasnetsov, Transformation of higher-order optical vortices upon focusing by a astigmatic lens, Opt. Commun. **241**, 237 (2004).

[49] J. W. Goodman, *Introduction to Fourier Optics* (McGraw Hill, New York, 1996), 2nd ed.

[50] Z. H. Pang, X. Y. Zhou, Z. L. Liu, and D. M. Zhao, Partially coherent quasi-Airy beams with controllable acceleration, Phys. Rev. A **102**, 063519 (2020).

[51] W. X. Yan, Y. Gao, Z. Yuan, Z. Wang, Z. C. Ren, X. L. Wang, J. P. Ding, and H. T. Wang, Non-diffracting and self-accelerating Bessel beams with on-demand tailored intensity profiles along arbitrary trajectories, Opt. Lett. **46**, 1494 (2021).

[52] Y. Wu, J. J. Zhao, Z. J. Lin, H. Q. Huang, C. J. Xu, Y. J. Liu, K. H. Chen, X. M. Fu, H. X. Qiu, H. Z. Liu, G. H. Wang, X. B. Yang, D. M. Deng, and L. L. Shui, Symmetric Pearcey Gaussian beams, Opt. Lett. **46**, 2461 (2021).

[53] Y. L. He, Z. X. Liu, Y. C. Liu, J. X. Zhou, Y. G. Ke, H. L. Luo, and S. C. Wen, Higher-order laser mode converters with dielectric metasurfaces, Opt. Lett. **40**, 5506 (2015).

[54] Y. Wu, C. J. Xu, Z. J. Lin, H. X. Qiu, X. M. Fu, K. H. Chen, and D. M. Deng, Abruptly autofocusing polycyclic tornado ring Airy beam, New J. Phys. **22**, 093045 (2020).

[55] Y. Wu, S. L. He, J. H. Wu, Z. J. Lin, L. B. Chen, H. X. Qiu, Y. J. Liu, S. H. Hong, K. H. Chen, X. M. Fu, Y. J. He, and D. M. Deng, Autofocusing Pearcey-like vortex beam along a parabolic trajectory, Chaos, Solitons Fractals **145**, 110781 (2021).

[56] H. X. Qiu, X. X. Lai, Y. Wu, H. Q. Huang, C. J. Xu, K. H. Chen, X. M. Fu, Z. J. Lin, D. M. Deng, and J. P. Guo, Effect of the spectral optical vortices on the chirped ring symmetric Airy beam, Opt. Commun. **499**, 127259 (2021).

[57] V. G. Shvedov, Y. V. Izdebskaya, A. V. Rode, A. Desyatnikov, W. Krolikowski, and Y. S. Kivshar, Generation of optical bottle beams by incoherent white-light vortices, Opt. Express **16**, 20902 (2008).

[58] A. Turpin, V. Shvedov, C. Hnatovsky, Y. V. Loiko, J. Mompart, and W. Krolikowski, Optical vault: A reconfigurable bottle beam based on conical refraction of light, Opt. Express **21**, 26335 (2013).

[59] See the Supplemental Material at http://link.aps.org/supplemental/10.1103/PhysRevApplied.17.054014, for the video for mesocarbon microbeads captured by TOBBs for about 3 minutes.

[60] Z. Zhang, D. Cannan, J. J. Liu, P. Zhang, D. N. Christodoulides, and Z. G. Chen, Observation of trapping and transporting air-borne absorbing particles with a single optical beam, Opt. Express **20**, 16212 (2012).

[61] Z. W. Mo, J. J. J. Q. F. Wei, D. L. Xu, H. B. Yang, H. Q. Huang, Y. Wu, H. Z. Liu, L. L. Shui, and D. M. Deng, Multiple and off-axis optical bottles from the chirped circular Pearcey Gaussian vortex beams, Opt. Express **30**, 1762 (2022).

[62] O. Jovanovic, Photophoresis-light induced motion of particles suspended in gas, J. Quant. Spectrosc. Radiat. Transf. **110**, 889 (2009).

[63] O. Jovanovic, Photophoresis-light induced motion of particles suspended in gas, J. Quant. Spectrosc. Radiat. Transf. **110**, 1762 (2009).

[64] Y. S. Liang, S. H. Yan, Z. J. Wang, B. L. Yao, and M. Lei, Off-axis optical levitation and transverse spinning of metallic microparticles, Photon. Res. **9**, 2144 (2021).